Clusters, Radicals, and Ions; Environmental Chemistry

Selectivity in Electron Attachment to Water Clusters

Aude Lietard, and Jan R. R. Verlet

Just Accepted

1
2
3
4
5
6
7
8
9
10
11
12
13
14
15
16
17
18
19
20
21
22
23
24
25
26
27
28
29
30
31
32
33
34
35
36
37
38
39
40
41
42
43
44
45
46
47
48
49
50
51
52
53
54
55
56
57
58
59
60

Selectivity in Electron Attachment to Water Clusters

Aude Lietard, Jan R. R. Verlet*

Department of Chemistry, Durham University, Durham DH1 3LE, United Kingdom

ABSTRACT

Electron attachment onto water clusters to form water cluster anions is studied by varying the point of electron attachment along a molecular beam axis and probing the produced cluster anions using photoelectron spectroscopy. The results show that the point of electron attachment has a clear effect on the final distribution of isomers for a cluster containing 78 water molecules, with isomer I formed preferentially near the start of the expansion and isomer II formed preferentially once the molecular beam has progressed for several millimetres. These changes can be accounted for by the cluster growth rate along the beam. Near the start of the expansion, cluster growth is proceeding rapidly with condensing water molecules solvating the electron, while further along the expansion, the growth has terminated and electrons are attached to large and cold preformed clusters, leading to the isomer associated with a loosely bound surface state.

*j.r.r.verlet@durham.ac.uk

Low energy electron attachment to water leads to the formation of hydrated electrons, in which the excess electron is solvated much like an anion. From a fundamental chemical physics perspective, the hydrated electron represents an archetypical quantum solute. More generally, hydrated electrons are ubiquitous and have been extensively studied because of the important chemical roles they play in many branches of science including: radiation chemistry and biology; astrochemistry and atmospheric chemistry; water remediation; nuclear chemistry; electron transfer chemistry; and plasma chemistry, biology and medicine.[1–6] While generally considered as a bulk solute, many of the roles of the hydrated electron are in fact associated with interfacial processes, but much less is known about the structure, let alone the reactivity, of excess electrons at aqueous interfaces.[7–16]

To gain a fundamental understanding of electron solvation in water, isolated water cluster anions, $(H_2O)_n^-$, have received much attention from both experiment[7,17–23] and theory.[9,24–29] In these, the excess electron can adopt a number of binding motifs. For small clusters ($n < 11$), the electron's density is external to the cluster and IR action spectroscopy has determined the structure of many of these.[19,20] The key feature in these is the presence of a water molecule that points both its H atoms towards the electron cloud (so-called AA-binding), and this motif remains evident for $n \lesssim 20$.[19] However, also in this range, different isomers of the clusters were observed using photoelectron (PE) spectroscopy. Specifically, distinct isomers (isomers I, II and III) could be identified by their different vertical detachment energy (VDE).[7,22,23] A recent computational study has assigned a specific binding to two of these isomers (I and II); isomer I is associated with the AA-motif, while isomer II has a surface state with single H-atoms from a number of water molecules binding the excess electron.[29]

For larger clusters ($n \gtrsim 50$), two dominant classes of isomers were also observed and with similar labels (isomer I and II).[7] Extrapolation of the VDE of isomer I to infinite cluster

size yields a value of ~ 3.2 eV,[7,22] which is consistent with the VDE for the bulk hydrated electron.[30] A similar extrapolation for isomer II yields a much lower VDE of ~ 1.6 eV.[7] Isomer II has its excess electron predominantly localised external to the cluster, while isomer I, which has sub-populations of isomers (Ia and Ib),[22] has its electron bound more tightly with several water molecules around the electron-density. These have been assigned convincingly using electronic structure calculations.[25] For the large clusters ($n \gtrsim 50$), both isomer classes can exist depending on the conditions under which they were generated.[7] The production of isomer II over isomer I could be achieved by increasing the stagnation pressure of the supersonic expansion used to generate the clusters. Such an increase is associated with the formation of "colder" clusters. It was inferred, and later verified, that isomer II is metastable with respect to isomer I with a free energy barrier separating the two.[22,31] Hence, under cold cluster conditions, it was suggested that there is insufficient energy to overcome the isomerisation barrier following electron attachment, thus leading to an enhancement of isomer II. However, no further insight into the *formation* of the different isomers could be gleaned. While the temperature of the cluster to which the electron attaches is important, during a supersonic expansion, nucleation to form the clusters is also progressing. Nucleation occurs along the molecular beam through collisions, which are most prevalent at the start of the expansion. Hence, the cluster growth rate (and therefore size) is a function of the distance from the orifice of the expansion.[32,33] To explore the importance of nucleation on the formation of different isomers of $(H_2O)_n^-$, we present experiments in which the location of electron attachment is varied along the axis of a supersonic expansion of water vapour seed gas in an Ar buffer gas that is maintained at a constant pressure. Using PE spectroscopy, we probe how different binding motifs arise upon the addition of an electron to a water cluster at different nucleation stages.

The experiment has been described previously.[34–36] The key elements of the experiment are shown in Figure 1(a), with a specific focus on the relevant parts for the current application. Water clusters were produced in a supersonic expansion of the vapour pressure of D_2O seeded in Ar carrier gas (1.5 bar) that was generated using a pulsed valve (150 μm orifice) held at a temperature of 318 K, operating at 10 Hz and expanded into a vacuum chamber where its operating pressure is at $\sim 10^{-5}$ mbar. D_2O was used instead of H_2O because it was previously noted that isomer II could be more readily formed in clusters of the former,[7] but we have observed similar results using H_2O. The supersonic expansion was crossed by a focussed electron beam (300 eV). The primary electron beam predominantly ionises Ar atoms in the expansion, ultimately leading to a plasma with relatively low energy electrons. These secondary electrons attach onto water clusters to form $(D_2O)_n^-$. The electron beam was focussed to a beam diameter of < 1 mm, ensuring spatial control of the attachment.[36] Note, however, that the ensuing plasma propagates along the molecular beam, which can be visualised by the asymmetric luminescence of the plasma.[36] An ion packet with a given m/z was selected from the broad $(D_2O)_n^-$ distribution using an orthogonal Wiley-McLaren time-of-flight spectrometer.[18] At the focus of the mass-spectrometer (after a field-free flight of ~ 1.2 m) a mass-selected $(D_2O)_n^-$ cluster ion packet was photodetached by a nanosecond light pulse from an Nd:YAG-pumped OPO operating at 425 nm. The resulting ejected PE were extracted perpendicularly using a velocity map imaging (VMI) spectrometer,[37] which records the PE velocity vectors in laboratory frame. The PE spectra were reconstructed from the raw images using the polar onion-peeling algorithm[38] and the VMI spectrometer's electron kinetic energy (eKE) scale was calibrated using the well-known atomic spectrum of I^-. The VMI spectrometer had a spectral resolution $\Delta eKE/eKE < 3\%$.[36]
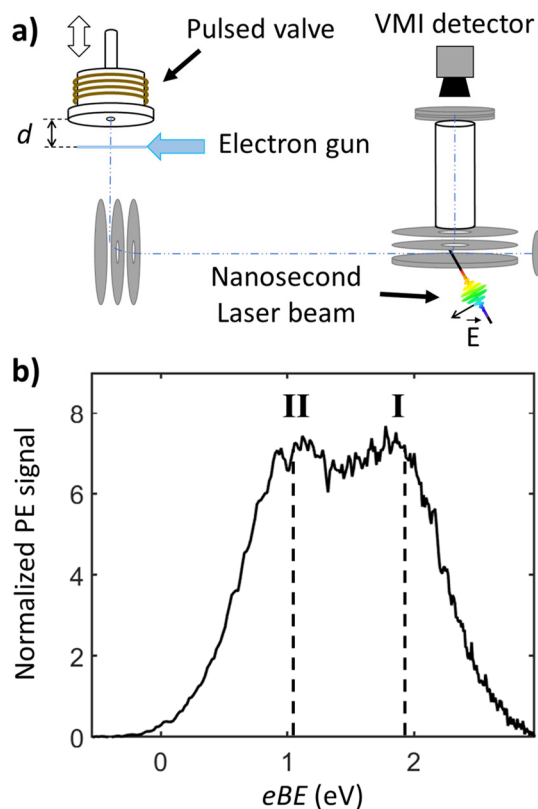
Figure 1: (a) Schematic of the experimental setup; (b) PE spectrum of $(H_2O)_{78}^-$ with peaks assigned to internally solvated and surface-localised electron isomers are labelled as I and II, respectively. The black dashed lines represent the VDE value of each isomer.

A typical PE spectrum of $(D_2O)_{78}^-$ is shown in Figure 1(b). The spectrum is broad and shows a bimodal distribution with two broad peaks labelled I and II. The PE spectra has been fitted using the known spectral profiles.[17,18] The peak labelled I has a VDE = 1.95 eV and that labelled II has a VDE = 1.10 eV: both are consistent with the VDE for this size measured previously.[7] For Figure 1(b), the supersonic expansion conditions (pressure and valve temperature) were optimised to produce roughly equal amounts of both isomers (assuming similar detachment cross-sections).

In order to select the location of the electron attachment during the cluster formation, the pulsed valve was mounted on a linear translator that allows us to move the valve along

the expansion propagation axis (Figure 1(a)). By changing the distance, d, between the valve

and the (fixed) electron gun beam, the location of where the electron beam crosses the

supersonic expansion could be controlled. Note that, given the molecular beam was pulsed,

specific care was taken to ensure that the same part of the molecular beam was extracted by

the time-of-flight optics following a calibration of the delay between the valve opening and

time-of-flight extraction.
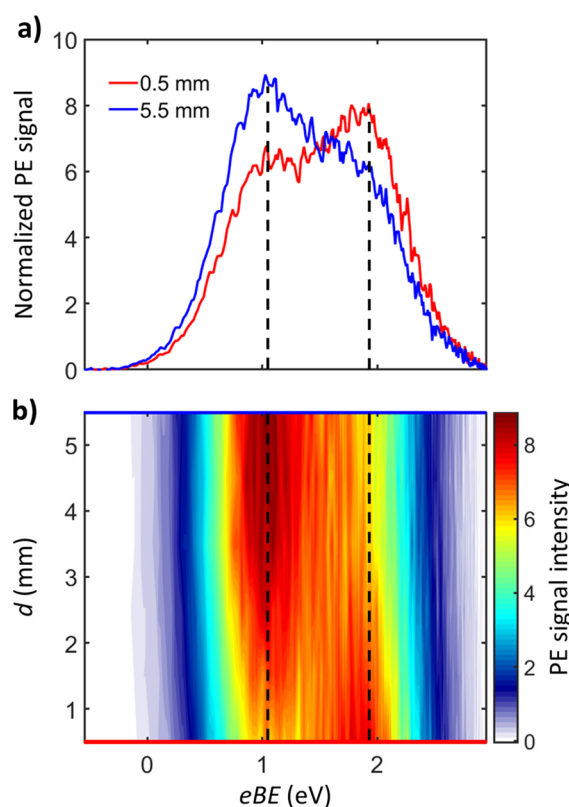
Figure 2: (a) PE spectra of $(D_2O)_{78}^-$ following electron attachment at $d \sim 0.5$ mm (red) and at $d \sim 5.5$ mm (blue), where d is the distance between the valve nozzle and the electron attachment point; (b) 2D representation of the $(D_2O)_{78}^-$ PE spectra as the function of d. PE spectra are normalised to total signal intensity. The black dashed lines represent the VDE position of the isomers I and II.

Figure 2 shows a series of PE spectra of $(D_2O)_{78}^-$ recorded as a function of d. Clear

changes are observed in the relative intensity of the two peaks as d changes. For electron

attachment near the start of the expansion, the dominant contribution to the PE spectrum is

from the higher binding isomer (isomer I), while the lower binding isomer (isomer II) is the

minor component. A representative PE spectrum (slice at $d \sim 0.5$ mm) is shown in

Figure 2(a). As the distance is increased, the relative contributions gradually change as

isomer II begins to contribute more and eventually dominates. After $d \sim 4$ mm, no further

changes are observed and the "asymptotic" PE spectrum (at $d \sim 5.5$ mm) is shown in

Figure 2(a). We note that we have observed similar control over isomeric distributions as a

function of d for other cluster sizes between $n \sim 50 - 100$ including for $(H_2O)_n^-$ clusters.

However, we have not performed a similarly detailed analysis for these.
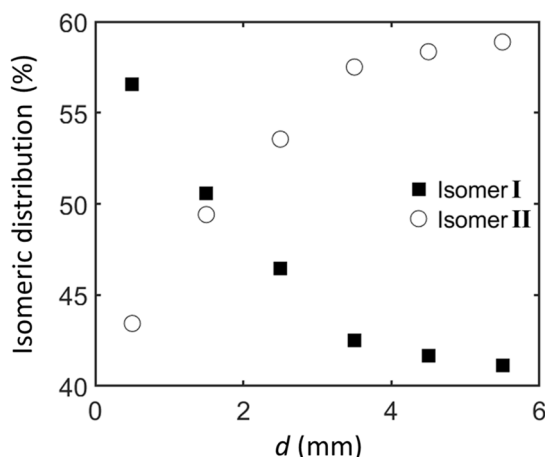
Figure 3: Relative contributions of isomers I and II as the function of the distance, d, between the pulsed valve nozzle and the electron attachment point.

To analyse the variation of the isomeric distribution with d, we have calculated the

relative contributions $R_I = I_I / (I_I + I_{II})$ and $R_{II} = I_{II} / (I_I + I_{II})$, where I_i is the integrated PE

signal of isomer i, by fitting the PE spectra using the known profiles.[17,18] The results of such

an analysis are shown in Figure 3. The graph represents the variation of the relative

contribution of the two isomers to the total ion packet as a function of d and clearly indicates

that these relative contributions change rapidly over the first 4 mm before reaching an

asymptotic distribution. For electron attachment at the start of the expansion (*i.e.* small d), the

majority of the $(D_2O)_{78}{}^-$ ion packet is isomer I; for electron attachment at large d, isomer II dominates with an asymptotic ratio of $\sim 60\ \%$. It is difficult to quantify the dominance of isomer I at small d because of the finite width of the electron beam and the fact that the plasma propagates along the beam axis for a short distance. Hence, the R_I values at very small d are likely to be under estimated.

The population inversion of isomers I and II as a function of d shown in Figures 2 and 3 clearly demonstrates that electron solvation in the water cluster is strongly influenced by the location of the electron attachment in the expansion. In molecular beam expansions, the cluster growth rate and internal temperature depend sensitively on the distance from the orifice (usually defined as a scaled distance relative to the orifice size), if other parameters such as the backing pressure, the source temperature, the carrier gas and the nozzle diameter are held constant.[32,33] The primary step in the cluster growth is the condensation of monomers to form dimers through "2+1" body collisions: two D_2O molecules combine to form the energised dimer $(D_2O)_2{}^*$, which may then either dissociate or undergo a collision with a third body (Ar in the present case) that quenches the excess energy to form the stable dimer $(D_2O)_2$.[32] Additional monomers can condense onto the dimer or dimers can condense onto each other in similar collision processes, ultimately leading to the growth of the cluster. Collision with the carrier gas leads to cooling; the carrier gas effectively acts as a refrigerant for the clusters. Hence, cluster growth at the early stages of the expansion is a balance between growth, which involves the increase of internal energy (temperature) of the $(D_2O)_n$ cluster, and cooling by collisions with Ar or evaporation of monomers. The transition between the free jet expansion and the molecular beam happens when no further collisions occur. This transition takes place when the terminal Mach number, $\mathcal{M}_T$, is reached.[39–41] For a seeded beam with low concentration of the seed gas, the behaviour of the expansion is effectively determined by the carrier gas. For an Ar expansion and assuming ideal gas

behaviour, it has been shown that $\mathcal{M}_T = 1.17(2^{1/2}\sigma\rho_0 D)^{0.4}$, where σ is the collision cross section, ρ_0 the Ar density in the source reservoir, and D the nozzle diameter.[41] Under the current experimental conditions, $\mathcal{M}_T$ is reached at a distance $d = 4.3$ mm.[40] Beyond this, we may expect that the cluster growth has terminated and the internal cluster temperature no longer changes. Although this analysis is rather crude, it does show remarkable agreement with the observed convergence to the "asymptotic" isomer distributions. We refrain from commenting on the internal temperature of the cluster as this is difficult to quantitatively predict, especially for clusters with many degrees of vibrational freedom.

With reference to Figure 4(a), the following picture of electron attachment emerges. When an electron is attached near the start of the expansion (*i.e.* small d), it is likely to be onto relatively small clusters, $(D_2O)_{n \ll 78}^-$. Although such clusters generally have their electron localised on the surface,[19,20] when additional water molecules (or small clusters) condense onto the $(D_2O)_{n \ll 78}^-$ cluster, they are likely to attach near the electron site of the initial $(D_2O)_{n \ll 78}^-$ cluster because of the stronger electron-dipole than dipole-dipole interactions. Furthermore, condensation increases the internal energy of the cluster, which enables isomerisation. Hence, for small d, one may anticipate that the formation of isomer I is favoured. For large d, nucleation has terminated and the electron is attached to a cold preformed $(D_2O)_{78}^-$ cluster. As schematically shown in Figure 4(b), the electron attaches to the surface of the cluster and, if there is insufficient internal energy to isomerise, it will remain there leading to a relative increase in isomer II. Although our results do not probe the electron binding motif directly, they indirectly support the idea that isomer I is associated with a more internalised electron distribution (embryonic hydrated electron) and isomer II with a surface-bound electron.
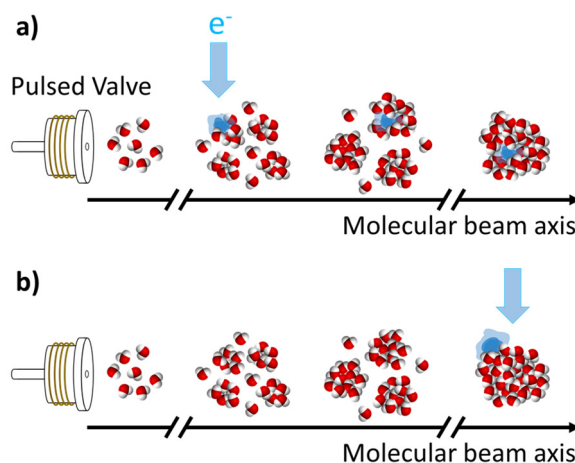
Figure 4: Schematic of electron attachment process at: (a) start of the expansion where the electron attaches to small clusters which subsequently grows with the condensation of additional water monomers and clusters; (b) the late stages of the expansion where the electron attaches to a cold preformed large cluster which does not have enough energy to isomerise. Argon atoms are omitted for simplicity.

The cluster-growth model for electron attachment presented here is closely linked to that suggested by Neumark and coworkers[7] in which formation of each isomer depends on the initial temperature of the cluster that was determined by the stagnation pressure. In their experiment, the point of electron attachment was fixed at $d \sim 7$ mm and the backing pressure of Ar increased to preferentially form isomer II over I. Higher pressure leads to faster cluster growth rates and more rapid cooling. This, in combination with the large d enabled the observation of isomer II, where the cluster growth has essentially terminated. In computational work, only the temperature effect has so far been considered and how this leads to the formation of different isomers. Our work suggests that the condensation of water molecules on small $(H_2O)_n^-$ clusters should also be considered.

In conclusion, we have shown that the location of electron attachment in a molecular beam expansion of water vapour in Ar carrier gas strongly influences the final electron solvation motif of an electron on a $(D_2O)_n^-$ cluster (with $n = 78$). The results imply that, in addition to the temperature of the cluster, the clustering dynamics occurring at the early stages of a supersonic expansion are an important factor in determining the solvation motif. The metastable isomer II cluster can be formed preferentially under cold (high carrier gas pressure) conditions and with electron attachment downstream from the supersonic expansion. The effect of condensation of water molecules on the final binding motif of $(H_2O)_n^-$ clusters may have important consequences on the likelihood of finding surface bound (isomer II) clusters in certain environments such as on interstellar ices or in the atmosphere.

REFERENCES

(1)   Bruggeman, P. J.; Kushner, M. J.; Locke, B. R.; Gardeniers, J. G. E.; Graham, W. G.; Graves, D. B.; Hofman-Caris, R. C. H. M.; D Maric; Reid, J. P.; Ceriani, E.; et al. Plasma–Liquid Interactions: A Review and Roadmap. *Plasma Sources Sci. Technol.* **2016**, *25*, 053002.

(2)   Garrett, B. C.; Dixon, D. A.; Camaioni, D. M.; Chipman, D. M.; Johnson, M. A.; Jonah, C. D.; Kimmel, G. A.; Miller, J. H.; Rescigno, T. N.; Rossky, P. J.; et al. Role of Water in Electron-Initiated Processes and Radical Chemistry: Issues and Scientific Advances. *Chem. Rev.* **2005**, *105*, 355–390.

(3)   Herbert, J. M.; Coons, M. P. The Hydrated Electron. *Annu. Rev. Phys. Chem.* **2017**, *68*, 447–472.

(4)   Schuler, R. H. Radiation Chemistry at Notre Dame 1943–1994. *Radiat. Phys. Chem.* **1996**, *47*, 9–17.

(5)   Buxton, G. V.; Greenstock, C. L.; Helman, W. P.; Ross, A. B. Critical Review of Rate Constants for Reactions of Hydrated Electrons, Hydrogen Atoms and Hydroxyl Radicals (·OH/·O− in Aqueous Solution. *J. Phys. Chem. Ref. Data* **1988**, *17*, 513–886.

(6)   Alizadeh, E.; Sanche, L. Precursors of Solvated Electrons in Radiobiological Physics and Chemistry. *Chem. Rev.* **2012**, *112*, 5578–5602.

(7)   Verlet, J. R. R.; Bragg, A. E.; Kammrath, A.; Cheshnovsky, O.; Neumark, D. M. Observation of Large Water-Cluster Anions with Surface-Bound Excess Electrons. *Science* **2005**, *307*, 93–96.

(8)   Uhlig, F.; Marsalek, O.; Jungwirth, P. Electron at the Surface of Water: Dehydrated or Not? *J. Phys. Chem. Lett.* **2013**, *4*, 338–343.

(9)   Barnett, R. N.; Landman, U.; Scharf, D.; Jortner, J. Surface and Internal Excess Electron States in Molecular Clusters. *Acc. Chem. Res.* **1989**, *22*, 350–357.

(10)   Gahl, C.; Ishioka, K.; Zhong, Q.; Hotzel, A.; Wolf, M. Structure and Dynamics of Excited Electronic States at the Adsorbate/Metal Interface: C6F6/Cu(111). *Faraday Discuss.* **2000**, *117*, 191–202.

(11)   Matsuzaki, K.; Kusaka, R.; Nihonyanagi, S.; Yamaguchi, S.; Nagata, T.; Tahara, T. Partially Hydrated Electrons at the Air/Water Interface Observed by UV-Excited Time-Resolved Heterodyne-Detected Vibrational Sum Frequency Generation Spectroscopy. *J. Am. Chem. Soc.* **2016**, *138*, 7551–7557.

(12)   Madarász, Á.; Rossky, P. J.; Turi, L. Excess Electron Relaxation Dynamics at Water/Air Interfaces. *J. Chem. Phys.* **2007**, *126*, 234707.

12

(13)   Casey, J. R.; Schwartz, B. J.; Glover, W. J. Free Energies of Cavity and Noncavity

Hydrated Electrons Near the Instantaneous Air/Water Interface. *J. Phys. Chem. Lett.*

2016, *7*, 3192–3198.

(14)   Siefermann, K. R.; Liu, Y.; Lugovoy, E.; Link, O.; Faubel, M.; Buck, U.; Winter, B.;

Abel, B. Binding Energies, Lifetimes and Implications of Bulk and Interface Solvated

Electrons in Water. *Nat. Chem.* **2010**, *2*, 274–279.

(15)   Sagar, D. M.; Bain, C. D.; Verlet, J. R. R. Hydrated Electrons at the Water/Air

Interface. *J. Am. Chem. Soc.* **2010**, *132*, 6917–6919.

(16)   Nowakowski, P. J.; Woods, D. A.; Verlet, J. R. R. Charge Transfer to Solvent

Dynamics at the Ambient Water/Air Interface. *J. Phys. Chem. Lett.* **2016**, *7*, 4079–

4085.

(17)   Coe, J. V. Fundamental Properties of Bulk Water from Cluster Ion Data. *Int. Rev.*

Phys. Chem. **2001**, *20*, 33–58.

(18)   Coe, J. V.; Williams, S. M.; Bowen, K. H. Photoelectron Spectra of Hydrated Electron

Clusters vs. Cluster Size: Connecting to Bulk. *Int. Rev. Phys. Chem.* **2008**, *27*, 27–51.

(19)   Asmis, K. R.; Santambrogio, G.; Zhou, J.; Garand, E.; Headrick, J.; Goebbert, D.;

Johnson, M. A.; Neumark, D. M. Vibrational Spectroscopy of Hydrated Electron

Clusters$(H2O)15–50−$ via Infrared Multiple Photon Dissociation. *J. Chem. Phys.* **2007**,

126, 191105.

(20)   Hammer, N. I.; Shin, J.-W.; Headrick, J. M.; Diken, E. G.; Roscioli, J. R.; Weddle, G.

H.; Johnson, M. A. How Do Small Water Clusters Bind an Excess Electron? *Science*

2004, *306*, 675–679.

(21)   Zappa, F.; Denifl, S.; Mähr, I.; Bacher, A.; Echt, O.; Märk, T. D.; Scheier, P. Ultracold

Water Cluster Anions. *J. Am. Chem. Soc.* **2008**, *130*, 5573–5578.

13

(22) Ma, L.; Majer, K.; Chirot, F.; von Issendorff, B. Low Temperature Photoelectron

Spectra of Water Cluster Anions. *J. Chem. Phys.* **2009**, *131*, 144303.

(23) Coe, J. V.; Lee, G. H.; Eaton, J. G.; Arnold, S. T.; Sarkas, H. W.; Bowen, K. H.;

Ludewigt, C.; Haberland, H.; Worsnop, D. R. Photoelectron Spectroscopy of Hydrated

Electron Cluster Anions, (H2O)−n=2−69. *J. Chem. Phys.* **1990**, *92*, 3980–3982.

(24) Herbert, J. M.; Jacobson, L. D. Nature's Most Squishy Ion: The Important Role of

Solvent Polarization in the Description of the Hydrated Electron. *Int. Rev. Phys. Chem.*

2011, *30*, 1–48.

(25) Jacobson, L. D.; Herbert, J. M. Theoretical Characterization of Four Distinct Isomer

Types in Hydrated-Electron Clusters, and Proposed Assignments for Photoelectron

Spectra of Water Cluster Anions. *J. Am. Chem. Soc.* **2011**, *133*, 19889–19899.

(26) Herbert, J. M.; Head-Gordon, M. First-Principles, Quantum-Mechanical Simulations of

Electron Solvation by a Water Cluster. *Proc. Natl. Acad. Sci.* **2006**, *103*, 14282–14287.

(27) Uhlig, F.; Marsalek, O.; Jungwirth, P. Unraveling the Complex Nature of the Hydrated

Electron. *J. Phys. Chem. Lett.* **2012**, *3*, 3071–3075.

(28) Kumar, A.; Walker, J. A.; Bartels, D. M.; Sevilla, M. D. A Simple Ab Initio Model for

the Hydrated Electron That Matches Experiment. *J. Phys. Chem. A* **2015**, *119*, 9148–

9159.

(29) Zho, C.-C.; Vlcek, V.; Neuhauser, D.; Schwartz, B. J. Thermal Equilibration Controls

H-Bonding and the Vertical Detachment Energy of Water Cluster Anions. *J. Phys.*

Chem. Lett. **2018**, *9*, 5173–5178.

(30) Luckhaus, D.; Yamamoto, Y.; Suzuki, T.; Signorell, R. Genuine Binding Energy of the

Hydrated Electron. *Sci. Adv.* **2017**, *3*, e1603224.

14

(31) Verlet, J. R. R.; Kammrath, A.; Griffin, G. B.; Neumark, D. M. Electron Solvation in Water Clusters Following Charge Transfer from Iodide. *J. Chem. Phys.* **2005**, *123*, 231102.

(32) Bourgalais, J.; Roussel, V.; Capron, M.; Benidar, A.; Jasper, A. W.; Klippenstein, S. J.; Biennier, L.; Le Picard, S. D. Low Temperature Kinetics of the First Steps of Water Cluster Formation. *Phys. Rev. Lett.* **2016**, *116*, 113401.

(33) Hagena, O. F. Nucleation and Growth of Clusters in Expanding Nozzle Flows. *Surf. Sci.* **1981**, *106*, 101–116.

(34) Rogers, J. P.; Anstöter, C. S.; Verlet, J. R. R. Ultrafast Dynamics of Low-Energy Electron Attachment via a Non-Valence Correlation-Bound State. *Nat. Chem.* **2018**, *10*, 341–346.

(35) Mensa-Bonsu, G.; Tozer, D. J.; Verlet, J. R. R. Photoelectron Spectroscopic Study of I−·ICF3: A Frontside Attack SN2 Pre-Reaction Complex. *Phys. Chem. Chem. Phys.* **2018**. DOI: 10.1039/C8CP06593D.

(36) Rogers, J. P.; Anstöter, C. S.; Bull, J. N.; Curchod, B. F. E.; Verlet, J. R. R. Photoelectron Spectroscopy of the Hexafluorobenzene Cluster Anions: $(C6F6)N−$ (n = 1 − 5) and $I−(C6F6)$. *J. Phys. Chem. A* **2019**. DOI: 10.1021/acs.jpca.8b11627.

(37) Eppink, A. T. J. B.; Parker, D. H. Velocity Map Imaging of Ions and Electrons Using Electrostatic Lenses: Application in Photoelectron and Photofragment Ion Imaging of Molecular Oxygen. *Rev. Sci. Instrum.* **1997**, *68*, 3477–3484.

(38) Roberts, G. M.; Nixon, J. L.; Lecointre, J.; Wrede, E.; Verlet, J. R. R. Toward Real-Time Charged-Particle Image Reconstruction Using Polar Onion-Peeling. *Rev. Sci. Instrum.* **2009**, *80*, 053104.

(39) Lubman, D. M.; Rettner, C. T.; Zare, R. N. How Isolated Are Molecules in a Molecular Beam? *J. Phys. Chem.* **1982**, *86*, 1129–1135.

15

(40)   DePaul, S.; Pullman, D.; Friedrich, B. A Pocket Model of Seeded Supersonic Beams.

        J. Phys. Chem. **1993**, *97*, 2167–2171.

(41)   Anderson, J. B.; Fenn, J. B. Velocity Distributions in Molecular Beams from Nozzle

        Sources. *Phys. Fluids* **1965**, *8*, 780–787.

16

50x50mm (300 x 300 DPI)